EXAFS of Carbon Monoxide Oxidation on Supported Pt Fuel Cell Electrocatalysts

Stephanie Maniguet, Rebecca J. Mathew, and Andrea E. Russell*

Department of Chemistry, University of Southampton, Highfield, Southampton, SO17 1BJ, United Kingdom

Received: August 20, 1999; In Final Form: December 28, 1999

The potential dependence of the extended X-ray absorption fine structure (EXAFS) obtained at the Pt L_{III} absorption edge for a carbon supported Pt electrocatalyst exposed to carbon monoxide is presented. The data have been analyzed using the difference file method to separate the dominant contributions of the Pt neighbors from contributions to the EXAFS from the adsorbed species. The presence of adsorbed CO is clearly observed with a Pt−C distance of 1.85 Å at potentials less than 0.5 V vs RHE. Increasing the potential above 0.5 V resulted first in the removal of the adsorbed CO and at more positive potentials, e.g., 1.05 V, in the formation of an oxide layer, as evidenced by the presence of a Pt−O coordination shell at 2.00 Å. These results demonstrate that in situ EXAFS of supported Pt electrocatalysts may be used to probe adsorbate structures.

Introduction

Improvements in the CO tolerance of the anode in reformate and methanol fuel cells are key to the commercial viability of proton exchange membrane (PEM) fuel cells. CO is a common contaminant of the H_2 feedstock from reformate, with typical levels of 30−100 ppm. CO is also thought to be the main poisoning species in methanol oxidation, formed as a strongly adsorbed partial oxidation product. The electrocatalysts for the anode are usually carbon supported Pt or Pt based alloys, such as Pt−Ru. The adsorption and electro-oxidation of CO on Pt electrodes and supported Pt electrocatalysts is, therefore, of considerable interest, both in relation to PEM fuel cell applications as well as a model adsorbate system.

Numerous spectroscopic methods have been employed to investigate the CO_{ads}/Pt system. In situ infrared spectroscopy has proved particularly useful,[1,2] enabling the identification of adsorption sites of CO, linear, bridged, or multifold adsorption and providing a means of estimating coverage as well as the structure of the adsorbate layer. Recent combined electrochemical scanning tunneling microscopy (STM) and in situ infrared studies have indicated that the full coverage CO_{ads}/Pt(111) phase is compressed with respect to that observed in UHV[3]. Most such in situ infrared studies, however, have been conducted using smooth, and more recently single crystal, Pt surfaces. In contrast, the carbon supported Pt in the electrocatalysts exists as small, 2−5 nm diameter, metal particles. Such small metal particles will have many surface atoms which correspond to step and edge sites. The adsorption and electro-oxidation of CO on such "rough" surfaces are likely to be different than on the smooth Pt surfaces. Two groups have recently reported in situ infrared studies using small metal particles. Friedrich and co-workers investigated CO adsorption on Pt particles dispersed on a gold substrate.[4] They found that the ν(C−O) stretching frequency for CO_{ads} depended on the particle size. However, they were not able to fully attribute this variation or the change in frequency with CO_{ads} coverage to changes in coordination of the adsorbate or lateral dipole field and concluded that some particle−substrate interaction must be present. Christensen et al. have conducted an investigation of methanol oxidation at small Pt particles dispersed on a basal plane graphite disc.[5] By comparing the results obtained with a bulk Pt electrode to those obtained with the Pt particles, they concluded that the electro-oxidation of methanol was sensitive to the morphology of the Pt surface; with methanol chemisorption occurring at more negative potentials on the particles and the coordination of CO_{ads} being 3-fold on the particles rather than the predominant singly bound species observed at bulk Pt.

In contrast to infrared measurements, in situ X-ray absorption spectroscopy (XAS) provides the ability to investigate the properties of the Pt electrocatalyst particles under conditions which more closely resemble those in the actual fuel cell environment. The XAS spectrum can be divided into two basic regions: the near edge region, termed the XANES (X-ray absorption near edge structure), and the EXAFS region (extended X-ray absorption fine structure). In in situ electrochemical studies of electrocatalysts, the former is useful in identifying oxidation states and the fractional d-electron density of the particles, while the latter provides more detailed structural information by probing the average nearest neighbor coordination of the Pt atoms in the particles. The EXAFS region provides information regarding the particle size and composition (number of neighbors), lattice contractions (coordination distance), and particle−substrate or particle−adsorbate interactions. Mukerjee and McBreen[6] have recently shown that the XANES region of the Pt L_{III} and L_{II} absorption edges for Pt particles less than 5 nm in diameter are sensitive to the chemisorption of hydrogen, hydroxide, and methanol. Here we report an EXAFS study of the chemisorption and electro-oxidation of CO on C supported Pt.

Experimental Section

Electrode. An appropriate quantity of 40 wt % Pt/XC-72R catalyst (supplied by Johnson Matthey, the preparation of which has been previously reported[7]) was suspended in Nafion and water to form an ink-like paste. The paste was stirred for 15 min and then spread onto carbon paper (E-Tek TGHP-120). The sheet was pressed at 14 kg cm^{-2} for 20 s at room temperature. Electrodes of area 2.54 cm^2 were cut from the compressed sheet for the in situ EXAFS measurements. Electrodes were boiled

* To whom correspondence should be addressed.

10.1021/jp992947x CCC: $19.00
Published on Web 02/10/2000

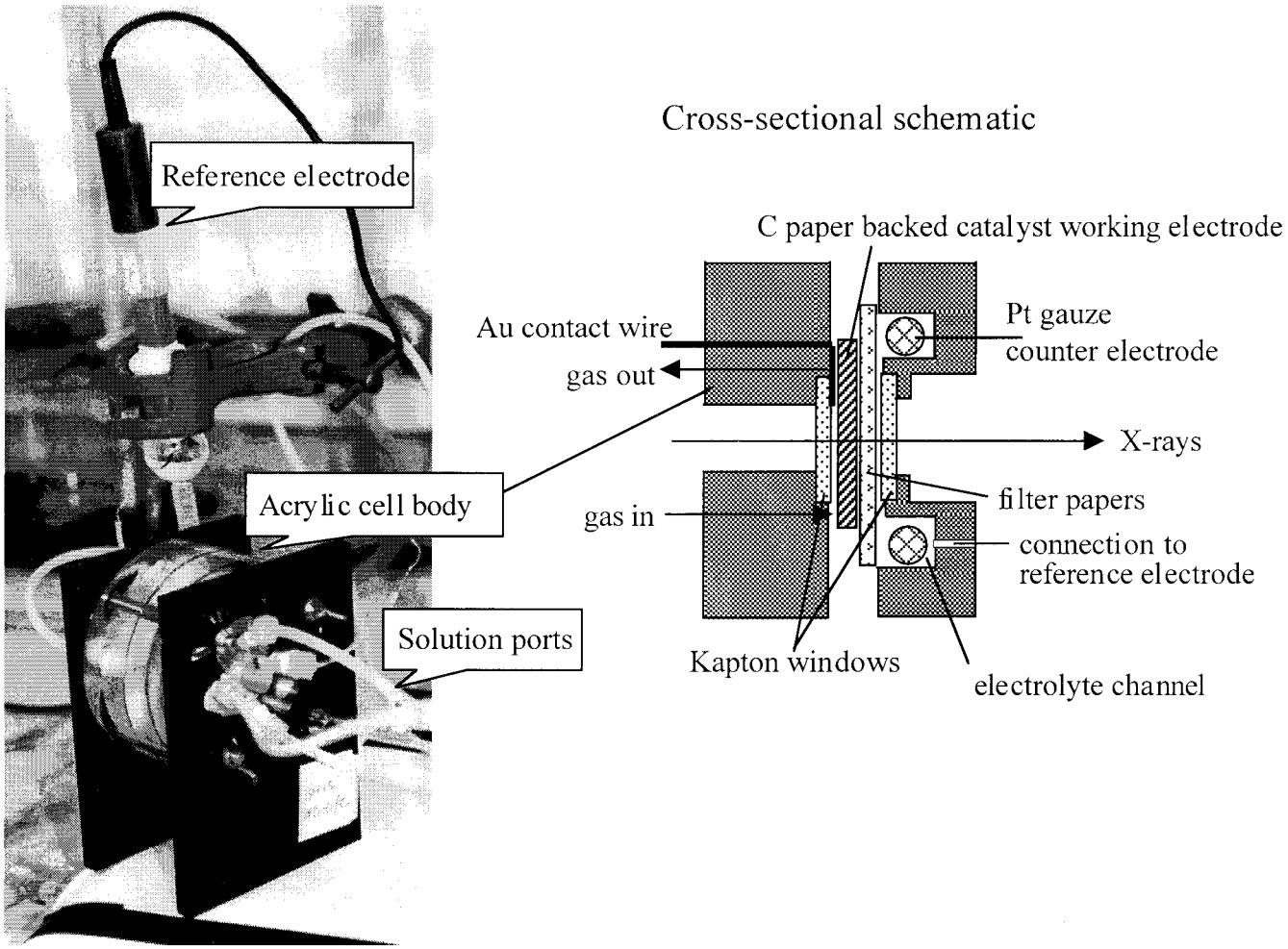

Figure 1. In situ XAFS cell for transmission data collection.

in triply distilled water prior to EXAFS studies to ensure a fully flooded state.

X-ray Absorption Fine Structure (XAFS) Measurements. The in situ transmission XAFS cell is shown in Figure 1 and is based on the design of Herron et al..[8] The carbon paper backed catalyst working electrode was placed against a gold wire current collector and several layers of filter paper soaked in electrolyte, 1.0 mol dm^{-3} H_2SO_4 prepared with 18 MΩ cm water, were placed over the electrode. This assembly was compressed between the two acrylic disks which made up the cell body. The X-rays entered and left the cell via Kapton windows. The electrolyte was flowed through the cell continuously during the experiments to remove gas bubbles and to ensure uniform composition of the thin layer of electrolyte in the cell. The electrode was exposed to CO by purging the gas through the composite electrode for 15 min. The platinum gauze counter electrode was situated in the electrolyte, and the reference electrode was connected via a salt bridge filled with the electrolyte solution. All potentials were measured with respect to a Hg/Hg_2SO_4 (MMS) reference electrode, but have been corrected to the RHE (reference hydrogen electrode) scale, as determined by calibrating with respect to a dynamic hydrogen/Pt electrode.

All X-ray data were collected on Wiggler station 9.2 of the Synchrotron Radiation Source (SRS) at Daresbury Laboratory, UK. The ring operated with 2.0 GeV energy and 100−250 mA current. The station was operated with a Si(220) double crystal monochromator which was detuned to 50% intensity to minimize the presence of higher harmonics. Three ion chambers, optimized for the (platinum L_{III} edge, were used in series to measure the intensities of the incident beam, I_0, the beam transmitted by the sample, I_t, and the beam subsequently transmitted by a platinum foil, I_m. The Pt foil was used as an internal reference, enabling calibration of the X-ray beam energy.

EXAFS Data Analysis. The EXAFS data was analyzed by performing multiple shell fitting in *r*-space using the XDAP data analysis package.[9] Experimental references were used to obtain the backscattering phase shifts and amplitudes for the Pt−Pt and Pt−O contributions using a Pt foil and $Na_2Pt(OH)_6$, respectively, with the following crystallographic parameters: $N = 12$ and $R = 2.77$ Å, for the Pt foil, and $N = 6$ and $R = 2.05$ Å for the $Na_2Pt(OH)_6$. A theoretical Pt−C reference file was calculated using FEFF 3.1 (10), with the following parameters: $N = 4$, $R = 1.99$ Å, $\Delta\sigma^2 = 0.002$ Å^2, and $S_0^2 = 0.93$.

In conducting the analysis of the EXAFS data, various *k* weightings of the data and Fourier transforms were applied. k^1 weighting emphasizes the contributions of low *Z* (low atomic number) neighbors, such as oxygen and carbon, as the maximum in the backscattering amplitude from such neighbors occurs at low values of *k*. k^3 weighting emphasizes heavier neighbors, such as platinum, and has been used to confirm the quality of the fits when the Pt−Pt contributions had been isolated. k^2 weighting provides a compromise between these two extremes and has been used in isolating the first shell contributions prior

to the fitting. The quality of the overall fit was examined using both k^1 and k^3 weightings.

The various backscatterers were identified using the difference file technique.[11] Briefly, the dominant Pt−Pt contributions were fit and then this fit was subtracted from the data. The remaining contributions, Pt−C and/or Pt−O, could then be fit. The contributions from the smaller number of these low *Z* neighbors were much weaker than the contributions from the Pt neighbors. Care was taken in the background subtraction (preliminary processing of the XAS data to isolate the EXAFS portion of the spectrum) to ensure that the procedure was completed systematically. The background was removed by the use of cubic splines such that

$$\sum_{i=1}^{\mathrm{NPTS}} \frac{(\mu x_i - \mathrm{BCK}_i)^2}{\exp(-\mathrm{WE}k_i^2)} \leq \mathrm{SM} \qquad (1)$$

Where NPTS is the number of data points, μx_i and BCK_i are the absorption and background at point *i*, respectively, SM is the smoothing parameter, and WE is the weighting parameter. WE was kept constant at 0.075, and SM was optimized to provide a maximum in the amplitude of the k^1 and k^3 weighted Fourier transforms at the distance of the first shell peak, while minimizing the amplitude of the Fourier transform at $R < 1$ Å. Individual data sets were obtained from a single electrocatalyst electrode, and all the spectra were obtained in succession; that is, the cell was not removed from the beamline between measurements. All the fit parameters were then optimized together by restricting the number of free parameters in any given fitting iteration. The data and fit were then compared in *r*-space (Fourier transform), and variances in the imaginary and absolute parts were used to determine the fit quality as previously described by Mojet et al.[12] Models with variances in absolute and imaginary parts below 1% are considered to represent very good models for the experimental data. The errors in the fit parameters are estimated to be 5−10% in coordination number (*N*), 1% in distance (*R*), 5−10% in Debye−Waller factor ($\Delta\sigma^2$), and 10% in inner potential correction (ΔE_0).

Results

Cyclic Voltammetry. CO oxidative stripping voltammograms were obtained for the Pt/C fuel cell electrode in a standard (nonthin layer) three electrode cell by recording a potential sweep in the range 0.0−1.2 V vs RHE. The surface of the supported Pt particles was exposed to CO by bubbling CO directly through the deaerated solution for approximately 15 min while holding the potential at 0.05 V. The solution was then purged with N_2 to remove any dissolved CO prior to recording the voltammogram. A representative volammogram is shown in Figure 2. Similar voltammograms were obtained in the in situ XAFS cell with only a minor increase in the resistive background. During the first forward sweep (from 0.05 to 1.2 V), the peaks characteristic of hydrogen desorption were suppressed by the presence of adsorbed CO, indicating nearly full CO coverage. The peak at 0.6 V corresponds to the oxidative stripping of the adsorbed CO layer. On the second sweep the voltammogram returns to that observed in the absence of CO purging and corresponds to that of Pt in the base electrolyte.

EXAFS of CO Covered Pt/C Fuel Cell Electrode. Panels a and c of Figure 3 show the raw EXAFS data and, in panels b and d, the corresponding k^1 weighted Fourier transform obtained for the Pt/C fuel cell electrode at 0.05 V vs RHE when exposed to CO. The dashed line in panels a and b represents

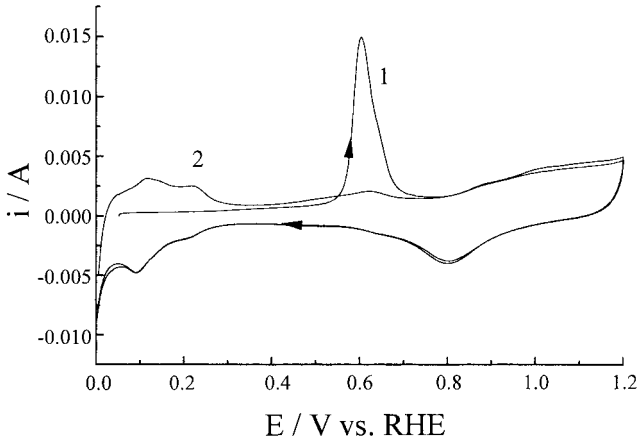

Figure 2. Cyclic voltammogram of Pt/C fuel cell electrode (electrode area 1 cm^2) in 1 mol dm^{-3} H_2SO_4. Electrode surface exposed to CO saturated solution while the potential was held at 0.05 V vs RHE. After adsorption, CO was displaced from solution by N_2 bubbling for 15 min. Sweep rate 20 mV s^{-1}. Numbers indicate peaks associated with first and second scans.

TABLE 1: Fit Parameters and Variances for Model Spectra for Pt/C with CO_{ads} at 0.05 V vs RHE

						k^0 variance (%)	
model	neighbor	N^a	R/Å (±1%)	$10^3\,\Delta\sigma^2$/Å (±5%)	ΔE_0/eV (±10%)	im part	abs part
1	Pt	9.39	2.76	3.7	2.1	0.07	0.06
	C	0.55	1.85	9.0[b]	9.0		
	C	1.36	2.71	9.0[b]	−13		
	C	1.91	3.70	9.0[b]	−13		
2	Pt	9.39	2.76	3.7	2.1	0.03	0.01
	Pt[c]	4.03	3.97	3.9	−12		
	C	0.60	1.85	9.0[b]	8.9		
	C	1.36	2.72	9.0[b]	−13		
	C	1.36	3.62	9.0[b]	−13		

[a] $N \pm 5\%$ for Pt−Pt shell and $N \pm 10\%$ for Pt−C shells. [b] Parameter fixed during fitting. [c] $N \pm 20\%$.

the best fit obtained after *r*-space analysis of the data after Fourier filtering chosen to include only the first Pt−Pt coordination distance; the filter conditions were k^2 weighted Fourier transform, $2 \leq k \leq 17$ Å^{-1}, $1.2 \leq r \leq 3.4$ Å. As described above, k^2 weighting was chosen to avoid overemphasis of the backscattering from either the low or high *Z* neighbors. The dots in panels c and d indicate the best fit obtained after *r*-space analysis of the data after Fourier filtering which included the second Pt−Pt coordination distance; the filter conditions were k^2 weighted Fourier transform, $2 \leq k \leq 17$ Å^{-1}, $1.1 \leq r \leq 4.0$ Å. The difference files which correspond to both fits are shown in Figure 4; panels a and c show the isolated data minus the fits of the C neighbors compared to the fit of the Pt neighbors, and panels b and d show the isolated data minus the fits of the Pt neighbors compared to the fit of the C neighbors. The parameters obtained for both fits are shown in Table 1.

The number of neighbors at the first Pt−Pt coordination distance is in fair agreement with the size of the Pt particles, determined by TEM (typical particle size 2−3 nm, with a distribution of particle diameters of 1−10 nm observed), if an icosahedral or cuboctahedral particle shape is assumed. It should be noted that the coordination number obtained from the EXAFS data is an average and, thus, does not reflect the distribution of particle sizes. Finely dispersed Pt particles which would be invisible in the TEM measurements would contribute to the EXAFS, decreasing the Pt−Pt coordination number. The particle sizes predicted by the first Pt−Pt coordination number in the

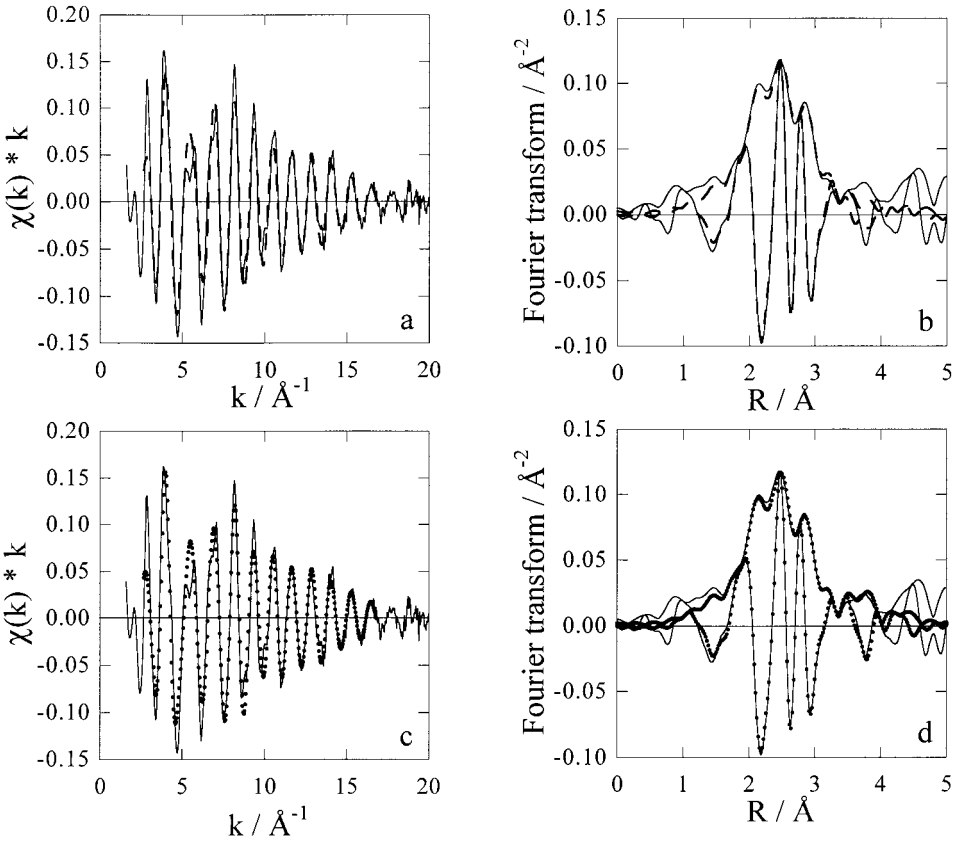

Figure 3. (a and c) k^1 weighted experimental data (not Fourier filtered) at 0.05 V vs RHE (solid line) and fits, including (a) only the first Pt−Pt distance (dashed line) and (c) both first and second Pt−Pt distances (dots), for Pt/C fuel cell electrode in 1 mol dm^{-3} H_2SO_4 following CO exposure. (b and d) k^1 weighted Fourier transforms, $3.1 \leq k \leq 14$ $Å^{-1}$, of the data and fits of spectra in (a) and (c), respectively.

EXAFS, therefore, are usually smaller than those obtained by TEM measurements.

The first Pt−C neighbor, at 1.85 Å, is attributed to the C of adsorbed CO and is in agreement with the distance obtained for CO adsorbed on zeolite supported Pt particles recently reported by Mojet et al.[12] as well as the ab initio cluster calculations recently presented by Curulla et al..[13] The remaining two Pt−C neighbors have previously been assigned to C from the support;[14,15] in the model previously reported, there are six C neighbors for each Pt atom at the particle/support interface. The effect of including the second Pt−Pt coordination distance does not significantly change the agreement between the fit and the data over the peaks in the Fourier transform corresponding to the first coordination shell, as seen in Figure 3. This is reflected in the minor variations in the fit parameters, with the only significant difference being in the third C neighbor shell. The decrease in the number of, and distance to, these neighbors may be related to the reduced effects of the tail of the second Pt−Pt neighbors when the Pt−Pt shell at 3.98 Å is included in the fitting.

Potential Dependence of the XAFS. Figure 5 shows the k^2 weighted Fourier transforms obtained as the applied potential was increased from 0.05 to 1.05 V vs RHE and then returned to 0.45 V. The Fourier transforms of the data obtained at 0.05 and 0.45 V prior to CO oxidation overlap, as do those at 0.65 V prior to oxide formation and 0.45 V after CO oxidation. The Fourier transform of the data obtained at 1.05 V exhibits the largest difference in amplitude and corresponds to the onset of oxide formation.

The first coordination shell was isolated by Fourier filtering as described above, with the filter range selected so as to exclude the second Pt−Pt coordination distance. The isolated data were then fit in *r*-space, as for the data collected at 0.05 V. Difference file plots illustrating the Pt−Pt and Pt−C or Pt−O contributions at several potentials are shown in Figure 6. The fit parameters are summarized in Table 2.

TABLE 2: Fit Parameters and Variances for Model Spectra for Pt/C as a Function of Potential

						k^0 variance (%)	
E/V vs RHE	neighbor	N^a	*R*/Å (±1%)	$10^3\,\Delta\sigma^2$/Å (±5%)	ΔE_0/eV (±10%)	im part	abs part
0.25	Pt	9.26	2.76	3.7	1.9	0.03	0.01
	C	0.43	1.85	9.0[b]	9.0		
	C	1.58	2.72	9.0[b]	−13		
	C	1.94	3.69	9.0[b]	−11		
0.45	Pt	9.23	2.76	3.6	1.3	0.03	0.01
	C	0.51	1.85	9.0[b]	9.0		
	C	1.44	2.71	9.0[b]	−13		
	C	2.32	3.71	9.0[b]	−12		
0.55	Pt	9.22	2.75	3.7	1.9	0.03	0.01
	C	1.45	2.66	4.0[b]	−9		
	C	2.14	3.32	9.0[b]	−11		
0.65	Pt	9.22	2.75	3.7	1.9	0.12	0.08
	C	1.63	2.64	4.0[b]	−8.9		
	C	2.32	3.30	9.0[b]	−11		
1.05	Pt	8.11	2.76	4.0	1.7	0.04	0.02
	O	0.75	2.00	2.9	13		
	C	2.15	2.64	4.0[b]	−10		
	C	3.97	3.24	9.0[b]	15		
0.45*	Pt	8.83	2.75	3.7	2.3	0.03	0.01
	C	1.56	2.64	4.0[b]	−9.0		
	C	1.53	3.55	9.0[b]	−5.8		

[a] $N \pm 5\%$ for Pt−Pt shells and ± 10% for Pt−C shells. [b] Parameter fixed during fitting.

The position and shape of the Fourier transform of the Pt component of the data (panels a, c, and e in Figure 6), does not

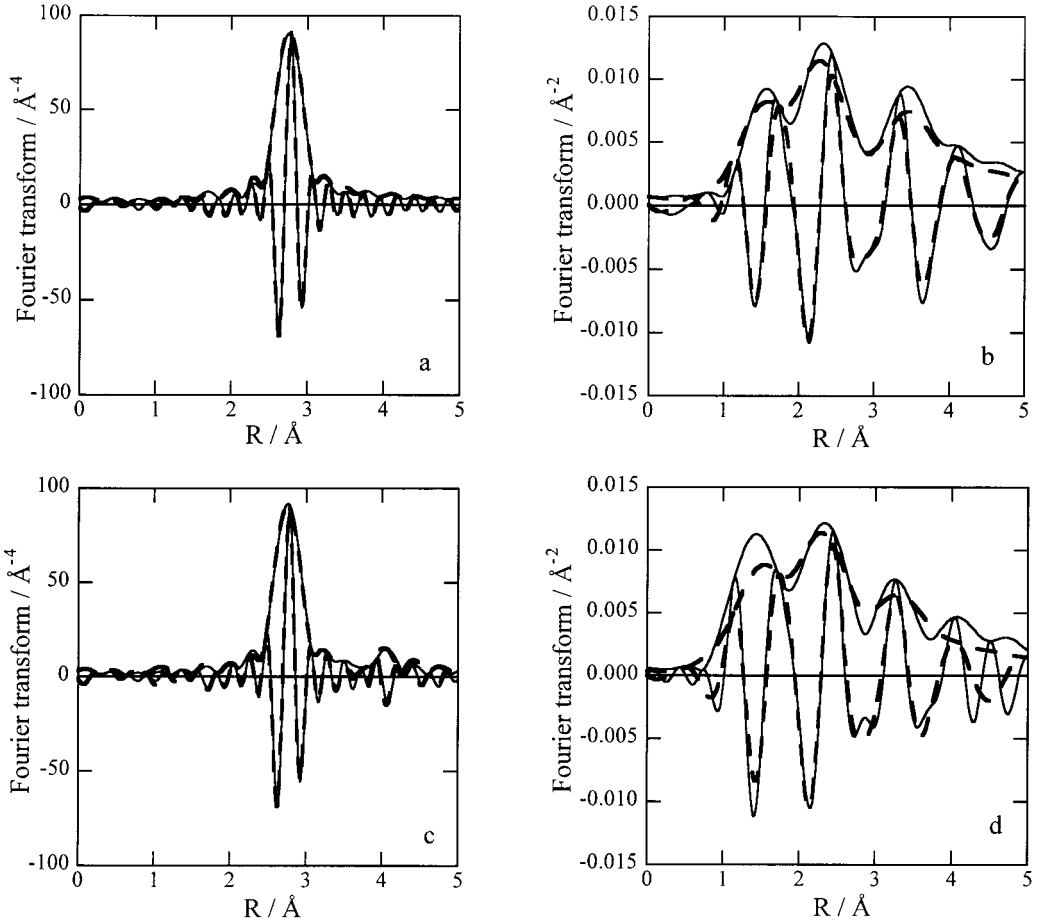

Figure 4. Difference plots corresponding to fits in Figure 3. (a and b) Fit including only the first Pt−Pt distance. (c and d) Fit including both first and second Pt−Pt distances. (a and c) k^3 weighted Fourier transform, $3.5 \leq k \leq 14$ Å^{-1}, Pt phase and amplitude corrected [isolated experimental EXAFS data-fit of C neighbors] (solid line) and fit of Pt neighbors (dashed line). (b and d) k^1 weighted Fourier transform, $3.5 \leq k \leq 9$ Å^{-1}, C phase corrected [isolated experimental EXAFS data-fit of Pt neighbors] (solid line) and fit of C neighbors (dashed line).

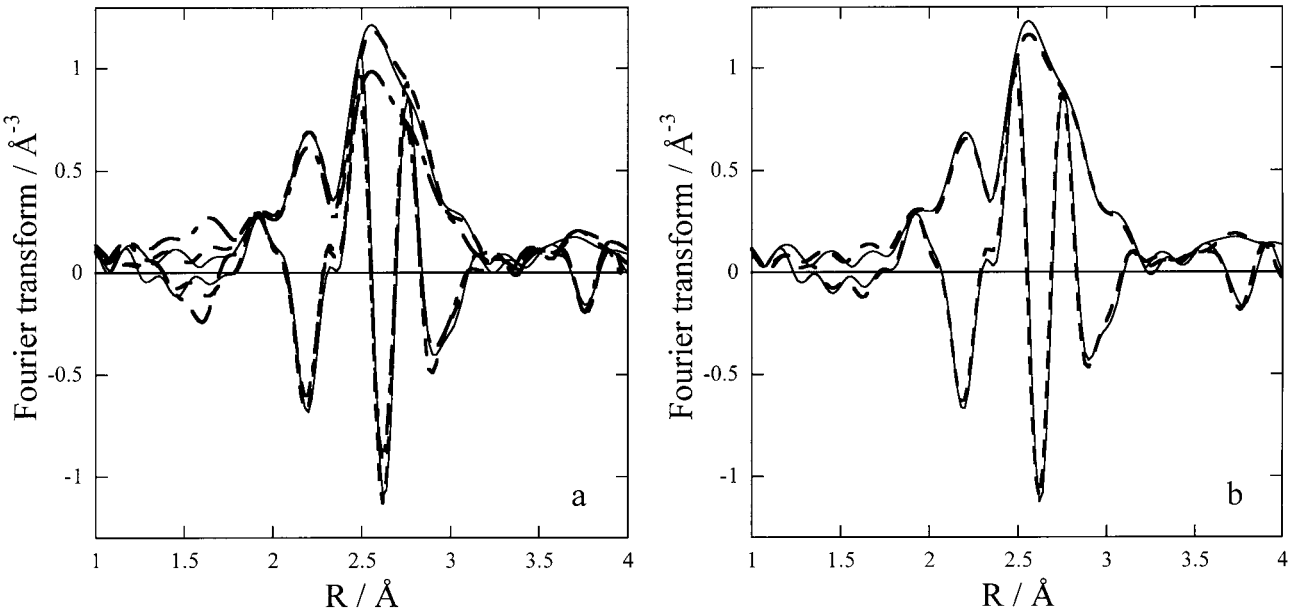

Figure 5. k^2 weighted Fourier transform, $3.1 \leq k \leq 14$ Å^{-1}, of the experimental EXAFS data of the CO exposed Pt/C electrode obtained at (a) 0.05 V (solid line), 0.65 V (dashed line), and 1.05 V (dot dashed line), note that the Fourier transforms of the 0.05 and 0.65 V data largely overlap, and (b) 0.45 V with adsorbed CO (solid line) and 0.45 V* after CO oxidation (dashed line). All potentials vs RHE.

change as a function of the applied potential. The amplitude of the Pt first coordination distance peak, however, decreased for the 1.05 V data, in agreement with previous EXAFS studies of oxide formation on Pt/C[6,16,17]. After reduction of the oxide, the amplitude recovered to nearly the same intensity observed prior to CO oxidation and oxide formation (compare panels a and e).

The presence of adsorbed CO and the formation of the oxide are more apparent in the difference file plots corresponding to the non-Pt neighbors (panels b, d, and f of Figure 6). The Fourier

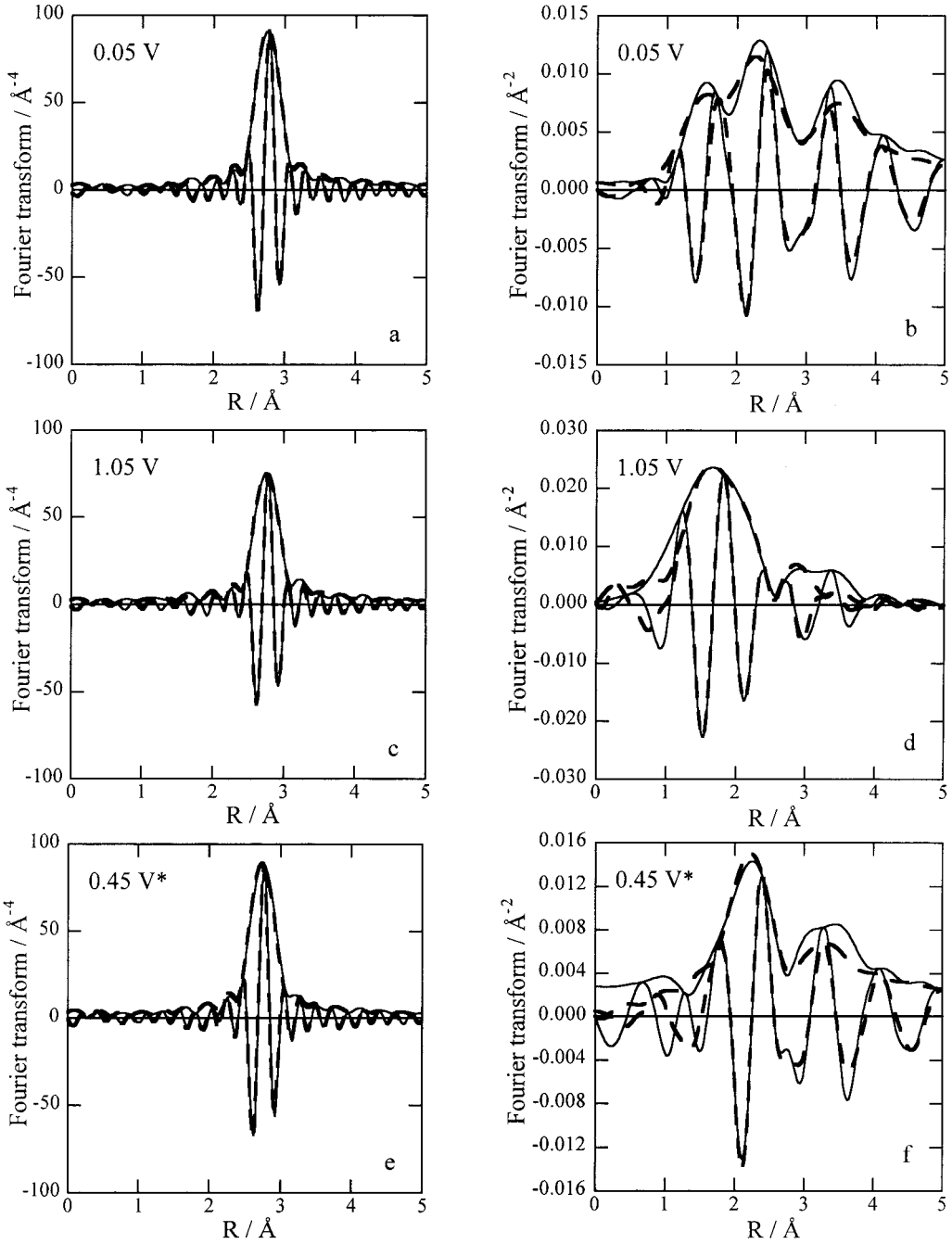

Figure 6. Difference plots as described in Figure 4 for the fits of the isolated first shells of the data obtained at (a and b) 0.05 V (CO adsorbate present), (c and d) 1.05 V (Pt surface oxidized), and (e and f) 0.45 V* (after CO oxidation). All potentials vs RHE.

transform at 0.05 V (panel b) is representative of the isolated data and fit for potentials more negative than 0.55 V, the onset of CO oxidation. The three peaks have been attributed to C neighbors of the adsorbed CO and two from the C support. At 1.05 V, the Pt particles are oxidized. The Fourier transform (panel d) is dominated by the O neighbors and has a shape which is very different from that when CO is adsorbed. Upon returning the potential to 0.45 V, the shape of the Fourier transform (panel f) again changes and the peaks may now be attributed to the C neighbors associated with the support.

Discussion

The EXAFS results indicate that the Pt particles are metallic in nature, both in the presence and absence of adsorbed CO, as evidenced by the Pt−Pt coordination number and distance. The results are consistent with previously reported XAS studies of carbon supported Pt fuel cell electrodes[4,15−17]. If an iscosahedral particle shape is assumed, the first-shell Pt−Pt coordiation number may be used to estimate the particle size. Using the formulas derived by Benfield,[18] an N of 8.51 corresponds to a 55 atom cluster, $N = 9.47$ a 147 atom cluster, and $N = 10.02$ a 309 atom cluster. The numbers of surface atoms for each of these cluster sizes are 42, 92, and 162, respectively. Adsorption of CO does not result in a change in the particle structure as indicated by the first Pt−Pt shell, in contrast to the reconstruction reported for CO adsorption on smaller (≤6 atoms) zeolite supported particles.[12] The lack of a significant change in the parameters of the first Pt−Pt shell is in agreement with restriction of the adsorbate layer to the surface of the Pt particles. The formation of the oxide at more positive potentials, however,

is not restricted to the surface of the particle as indicated by the decrease in the first Pt−Pt coordination number.

The Pt−C distance for adsorbed CO, 1.85 Å, is in good agreement with that reported for CO adsorbed on zeolite supported Pt particles, 1.92 Å. The Pt−C coordination number, 0.5, is in agreement with a monolayer of CO adsorbed on the surface of the Pt particles; N_{surf}/N_{total} is 0.45−0.63 for particle sizes corresponding to the first Pt−Pt coordination number. The large inner potential corrections observed for the other C shells, attributed to the Pt particle/C support interface, have previously been attributed to fitting several closely spaced Pt−C distances as one distance.[15,19] The large Debye−Waller factors also agree with this interpretation.

The Pt−C bond distances for adsorbed CO as determined in the ab initio calculations of Curulla et al.[13] are 1.86−1.90 Å for CO adsorbed at the on-top/linear site and 1.44−1.49 Å for CO adsorbed at the bridge bonded site, using a 29 Pt atom cluster. The Pt−C distance obtained in this investigation, 1.85 Å, therefore suggests that the CO is adsorbed linearly, although the presence of bridge bonded CO cannot be excluded. At potentials where CO is adsorbed, additional longer Pt−C and Pt−O distances will also be present. If the CO is assumed to be adsorbed linearly, then a Pt−O neighbor would be expected at 2.95 Å and a Pt−C neighbor at 3.32 Å. The presence of the C neighbors from the support make a statistically significant observation of the Pt−O bond distance for the adsorbed CO, reported at 2.86 Å for the zeolite supported Pt particles,[12] difficult. In addition, the backscattering phase shifts and amplitudes for the C and O neighbors are very similar. It is therefore, not feasible to investigate the influence of the applied electrode potential on the C−O bond length for C supported Pt particles. In situ infrared studies of CO adsorbed on smooth Pt surfaces have shown that the frequency of the ν(CO) stretching vibration is dependent on the applied electrode potential or electric field strength. This phenomenon, known at the electrochemical Stark effect, has been attributed to both a potential dependent change in the π-back-bonding between the Pt d electrons and the π^* antibonding orbital of adsorbed CO and a coupling of the dynamic dipole of the C−O bond with the electric field strength.[20,21] A change in the Pt−C and C−O bond lengths with applied potential was, therefore, anticipated. No change in the Pt−C distance was observed over the 0.05 to 0.45 V potential region investigated in this study.

Examination of the cyclic voltammogram, Figure 2, shows that at potentials above 0.55 V the CO is oxidized off the Pt surface and at potentials greater than 0.85 V the Pt surface is oxidized. This change in the surface composition of the Pt particles is clearly observed in the EXAFS; see Figure 6. In agreement with the cyclic voltammogram, the EXAFS data show that CO is removed prior to oxidation of the Pt particles. The inner potential correction and Debye−Waller factor for the Pt−C shell at 2.6 Å for the fits of the data obtained at 0.55 and 0.65 V are reduced in comparison to those where CO is adsorbed. At these potentials, where CO is removed, but prior to oxide formation, fewer closely spaced Pt−C distances are present.

Conclusion

This investigation has shown that in situ XAFS of fuel cell electrocatalysts is sensitive to the surface composition of the metal particles and may be used to investigate the chemistry of the fuel cell reactions. The use of the difference file method enables subtraction of the dominant Pt−Pt interactions and detailed examination of the remaining non-Pt neighbors. The EXAFS fit parameters obtained in this study are consistent with the adsorption of a monolayer of CO on the Pt particles. The presence of contributions to the EXAFS from the C neighbors of the support prevent the determination of the effect of the applied potential on the C−O bond length and independent discrimination between the various possible adsorption sites, e.g., linear, bridge, or multifold bonding.

Acknowledgment. The authors thank Johnson Matthey for the loan of the electrocatalyst materials, Fred Mosselmans and Chris Corrigan (Darebury Laboratory) for their assistance while at the SRS, and Gert van Dorssen, Jan de Graaf (University of Utrecht), Jun Yao, and Linda Carrette (University of Southampton) for their help and companionship at Daresbury Laboratory. R.J.M. acknowledges the support of the EPSRC through a Quota studentship. The project is jointly supported by the EPSRC (GR/L69817), MOD, and Johnson Matthey.

References and Notes

(1) Beden, B.; Bewick, A.; Kunimatsu, K.; Lamy, C. *J. Electroanal. Chem.* **1982**, *142*, 345.
(2) Iwasita, T.; Nart, F. C.; In *Advances in Electrochemical Science and Engineering*; Gerischer, H., Tobias, Ch., Eds.; Verlag: New York, 1995; Vol. 4.
(3) Gomez, R.; Feliu, J. M.; Aldaz, A.; Weaver, M. J. *Surf. Sci.* **1998**, *410*, 48.
(4) Friedrich, K. A.; Henglein, F.; Stimming, U.; Unkauf, W. *Colloids Surf. A* **1998**, *134*, 193.
(5) Christensen, P. A.; Hamnett, A.; Munk, J.; Troughton, G. L. *J. Electroanal. Chem.* **1994**, *370*, 251.
(6) Mukerjee, S.; McBreen, J.; *J. Electroanal. Chem*. **1998**, *448*, 163.
(7) Keck, L.; Buchanan, J.; Hards, G.; U.S. Patent 5,068,161, 1991.
(8) Herron, M. E.; Doyle, S. E.; Pizzini, S.; Roberts, K. J.; Robinson, J.; Hards, G.; Walsh, F. C. *J. Electroanal. Chem.* **1992**, *324*, 243.
(9) Supplied by XAFS Services International, The Netherlands, http://www.xs4all.nl/∼xsi.
(10) Rehr, J. J.; Albers, R. C.; Sabinsky, S. I. *Phys. Rev. Lett*. **1992**, *69*, 3397. Rehr, J. J.; Albers, R. C. *Phys. Rev. B* **1990**, *41*, 8139.
(11) Duivenvoorden, F. B. H.; Koningsberger, D. C.; Uh, Y. S.; Gates, B. C. *J. Am. Chem. Soc.* **1986**, *108*, 6254.
(12) Mojet, B. L.; Miller, J. T.; Koningsberger, D. C. *J. Phys. Chem. B* **1999**, *103*, 2724.
(13) Curulla, D.; Clotet, A.; Ricart, J. M.; Illas, F.; *J. Phys. Chem. B* **1999**, *103*, 5246.
(14) O′Grady, W. E.; Koningsberger, D. C. *Electrochem. Soc. Extended Abstr.* **1998**, *88* (1), 513.
(15) Lampitt, R. A.; Carrette, L. P. L.; Hogarth, M. P.; Russell, A. E. *J. Electroanal. Chem.* **1999**, *460*, 80.
(16) Weber, R. S.; Peuckert, M.; DallaBetta, R. A.; Boudart, M. *J. Electrochem. Soc.* **1988**, *135*, 2535.
(17) Allen, P. G.; Conradson, S. D.; Wilson, M. S.; Gottesfeld, S.; Raistrick, I. D.; Valerio, J.; Lovato, M.; *J. Electroanal. Chem*. **1995**, *384*, 99.
(18) Benfield, R. E.; *J. Chem. Soc., Faraday Trans.* **1992**, *88*, 1107.
(19) Mojet, B. L.; Hoogenraad, M. S., van Dillen, A. J.; Geus, J. W.; Koningsberger, D. C.; *J. Chem. Soc., Faraday Trans.* **1997**, *93*, 4371.
(20) Lambert, D. K. *Solid State Commun.* **1984**, *51*, 297.
(21) Holloway, S.; Norskov, J. K.; *J. Electroanal. Chem.* **1984**, *161*, 193.